Measurements of upper mantle shear wave anisotropy from a permanent network in southern Mexico

Steven A. C. van Benthem, Raúl W. Valenzuela* and Gustavo J. Ponce

Resumen

Se midió la anisotropía para las ondas de cortante en el manto superior por debajo de estaciones en el sur de México usando fases *SKS.* Las direcciones de polarización rápida donde la placa de Cocos se subduce subhorizontalmente están orientadas aproximadamente paralelas con el movimiento relativo entre las placas de Cocos y América del Norte y además son perpendiculares a la trinchera. Por lo tanto, se infiere que la placa subducida arrastra el manto que se encuentra por debajo y lo hace fluir (entrained flow). Una situación similar existe en la zona de subducción de Cascadia. Estudios previos han señalado que estas dos regiones tienen en común la subducción de litosfera joven. En aquellos lugares donde las placas subducidas muestran un cambio en el buzamiento o bien están rotas, se observa un cambio en la orientación de los ejes rápidos. Dichos cambios sugieren que se produce un flujo tridimensional alrededor de las orillas de las placas subducidas, el cual es consistente con el retroceso de la placa subducida (slab retreat or rollback), como ya se había observado en algunos trabajos anteriores. En algunas de las estaciones instaladas lejos de los límites de placa el movimiento absoluto de la placa de América del Norte controla las direcciones rápidas. El eje rápido de una estación ubicada en la Mesa Central se orienta ONO-ESE y es diferente de todas las demás mediciones en este estudio.

Palabras clave: Partición de ondas *SKS,* anisotropía del manto superior, flujo del manto, zonas de subducción, Fosa Mesoamericana, placas de Cocos, Rivera y América del Norte.

Abstract

Upper mantle shear wave anisotropy under stations in southern Mexico was measured using records of *SKS* phases. Fast polarization directions where the Cocos plate subducts subhorizontally are oriented in the direction of the relative motion between the Cocos and North American plates, and are trench-perpendicular. This pattern is interpreted as subslab entrained flow, and is similar to that observed at the Cascadia subduction zone. Earlier studies have pointed out that both regions have in common the young age of the subducting lithosphere. Changes in the orientation of the fast axes are observed where the subducting plates change dip and/or are torn, and are thus indicative of 3-D flow around the slab edges. They are consistent with slab rollback, as previously shown by other authors. Some stations located away from the plate boundaries have their fast directions controlled by the absolute motion of the North American plate. The fast axis for station ZAIG, located in the Mesa Central, is oriented WNW-ESE and is different from all the other measurements in this study.

Key words: *SKS* splitting, upper mantle anisotropy, mantle flow, subduction zones, Middle America Trench, Cocos, Rivera, and North American plates.

G. J. Ponce
Departamento de Sismología
Instituto de Geofísica
Universidad Nacional Autónoma de México
Circuito de la Investigación S/N
Cd. Universitaria
Del. Coyoacán
04510. México, D.F., México

Also at Departamento de Geofísica
Facultad de Ingeniería
Universidad Nacional Autónoma de México
Mexico D.F., México

R. W. Valenzuela*
Departamento de Sismología
Instituto de Geofísica
Universidad Nacional Autónoma de México
Circuito de la Investigación S/N
Cd. Universitaria
Del. Coyoacán
04510. México, D.F., México
*Corresponding author: raul@ollin.igeofcu.unam.mx

S. A. C. van Benthem
Department of Earth Sciences
Utrecht University
Budapestlaan 4, 3584 CD Utrecht
The Netherlands

Formerly at Departamento de Sismología
Instituto de Geofísica
Universidad Nacional Autónoma de México
Mexico D.F., México

Introduction

The use of the teleseismic phase *SKS* to study upper mantle anisotropy in both seismically quiet and seismically active regions has become a standard tool (Silver, 1996; Savage, 1999; Park and Levin, 2002). The method is based on the intrinsic anisotropy of the seismic velocity of the mineral olivine, which is one of the major components of the upper mantle. Olivine crystals become oriented as they are subjected to strain, usually caused by mantle flow. As the *SKS* phase travels through an anisotropic medium it becomes split, i. e. a fast and a slow wave are produced. Measurements of shear wave splitting yield two parameters: the fast polarization direction, ϕ, usually referred to geographic north, and the delay time, δt. Laboratory experiments are essential to establish the relationship between the direction of mantle flow and the fast polarization direction in olivine. In general, these experiments have shown that the fast axis becomes oriented in the direction of mantle flow (Jung *et al.*, 2006). There is one notable exception, for type-B olivine the fast axis aligns perpendicular to the direction of mantle flow. From these results it is possible to infer the direction of mantle flow using seismic measurements. Connections between seismic anisotropy and the tectonic environment, whether it be active margins or stable continental interiors, have been made in the past (e. g., Silver, 1996; Savage, 1999; Park and Levin, 2002). Particularly, subduction zones have come under intense scrutiny; see Long and Silver (2008, 2009) for a review. Previous work in the case of Mexico has relied mostly on data from temporary deployments and has focused around the Gulf of California (Obrebski *et al.*, 2006; Obrebski and Castro, 2008; van Benthem *et al.*, 2008; Long, 2010), and on subduction of the Rivera and Cocos plates at the Middle America Trench (Stubailo and Davis, 2007, 2012a, 2012b; Bernal-Díaz *et al.*, 2008; Soto *et al.*, 2009; Rojo-Garibaldi, 2012). In the present article, data from a permanent broadband network has been used, thus covering a large area of the country with widely spaced stations. This approach stands in contrast to temporary deployments which usually cover smaller areas with a dense array.

Data and Procedure

Most of the anisotropy measurements in this study used the *SKS* phase at epicentral distances greater than 90°. Additionally, other core-transmitted phases such as *sSKS, SKKS,* and *PKS* were used as available. Clear *SKS* readings at these distances required a minimum magnitude of 6.0, although occasionally smaller events proved useful. The records were provided by Mexico's Servicio Sismológico Nacional (SSN) broadband network (Singh *et al.*, 1997). The SSN database

was searched in the period from May 1998 to early January 2004. It provided a total of 359 earthquakes within the distance and magnitude criteria. Local problems with the equipment precluded the simultaneous recording of some events by all stations. The data were sampled 20 times per second using Streckeisen STS-2 broadband, three-component velocity sensors, except at station TEIG, where a Geotech KS36000 borehole seismometer was installed. Figure 1 shows the study area and the location of the 20 stations used.

The procedure used to measure anisotropy was explained by Silver and Chan (1991) and is presented here only briefly. The split *SKS* waves are observed in the fast and slow horizontal components, which are orthogonal. In general, these are different from the radial and transverse components, which are also orthogonal. In order to obtain ϕ and δt, a time segment containing the *SKS* arrival, or another *P* to *S* conversion at the core-mantle boundary (CMB), is selected from the north-south and east-west horizontal components. The two components are rotated by one degree at a time, with ϕ ranging between -90 and 90°. For each value of ϕ, the components are time shifted relative to each other using increments of 0.05 s, with δt ranging from 0 to 8 s. For each combination of ϕ and δt, the eigenvalues λ_1 and λ_2 of the covariance matrix between the two orthogonal components are evaluated. For an anisotropic medium, λ_1 and λ_2 will be different from zero. In the presence of noise, the desired solution will be given by the matrix which is most nearly singular. A grid search is then run through all combinations of (ϕ, δt) within the space of possible solutions in order to choose the minimum eigenvalue, λ_2^{min}. The actual values of (ϕ, δt) associated to λ_2^{min} characterize the anisotropy because the highest cross-correlation within the given space occurs for the fast and slow waveforms. Sometimes the measurement returns a null value and splitting of the shear wave cannot be detected, as is the case for any of the three following situations. (1) $\delta t =$ 0 s indicates the absence of anisotropy. (2) $\phi = \phi_b$ means that the fast axis, ϕ, is oriented with the back azimuth, ϕ_b. (3) $\phi = \phi_b + 90°$ means that the fast axis is perpendicular to the back azimuth.

Figure 2a shows the *SKS* arrival on the radial and transverse components at SSN station OXIG for the earthquake of May 16, 1998 south of the Fiji Islands. The hypocenter was located at 586 km depth and the epicentral distance was 90.10°. Table 1 lists the events used in this study to quantify upper mantle anisotropy. Each *SKS* waveform was chosen by visual inspection and a first order, bandpass Butterworth filter was applied. In every case an attempt was made to retain the broadest bandpass possible, but the actual corner frequencies were determined
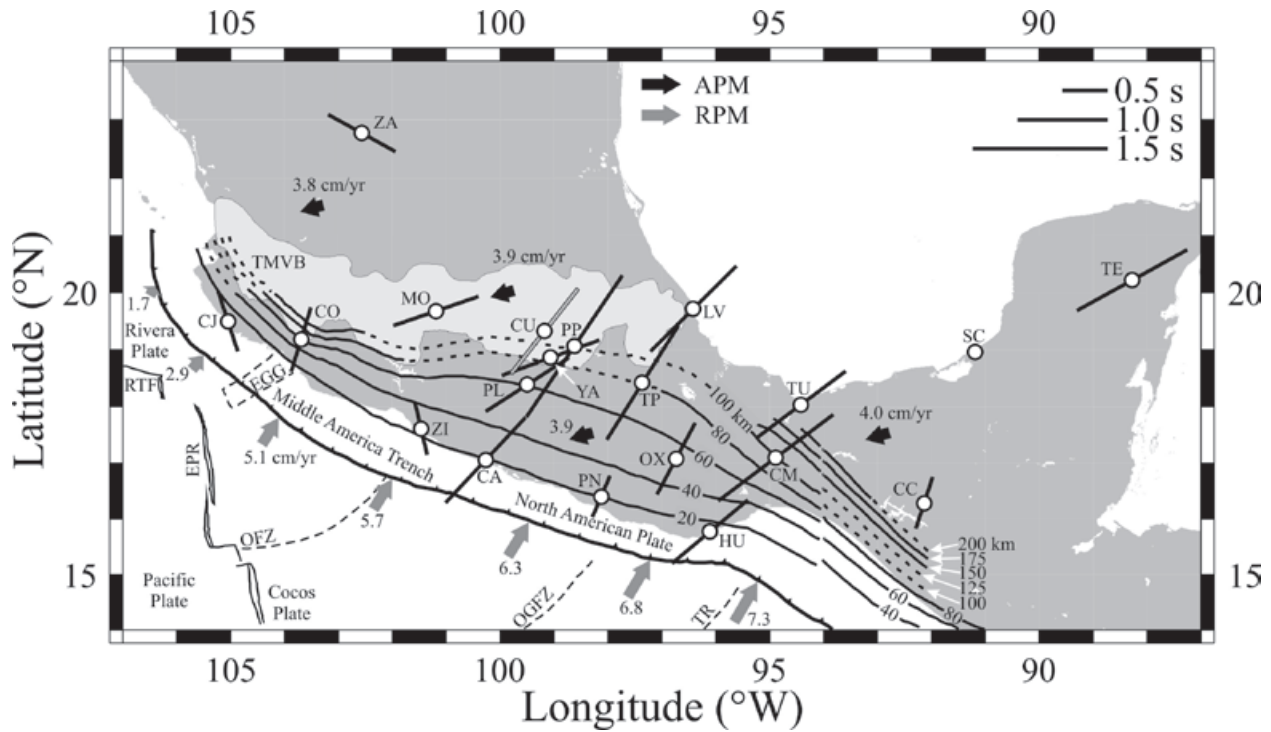
Figure 1. Average measurements of ϕ and δt for stations in southern Mexico. The length of the black bars is proportional to δt, as indicated in the legend. The gray bar at CUIG represents a poorly constrained measurement. Black arrows indicate the direction of absolute motion for the North American plate. Gray arrows show the direction of the relative plate motions for either the small Rivera (northwest) or the larger Cocos (southeast) plate relative to North America. Velocities are given in cm/yr for both the APM and the RPM. The Middle America Trench is represented by the line with small triangles. The Trans-Mexican Volcanic Belt (TMVB) is indicated by the light shading. Solid lines represent the isodepth contours of hypocenters within the subducting Rivera and Cocos plates. Lines are dashed where no hypocenters were available. Contours west of 94°W are from Pardo and Suárez (1995) while contours east of 94°W are from Rodríguez-Pérez (2007). In all cases, contours deeper than 100 km are from Rodríguez-Pérez (2007). Also shown are the Rivera Transform Fault (RTF), East Pacific Rise (EPR), El Gordo Graben (EGG), Orozco Fracture Zone (OFZ), O'Gorman Fracture Zone (OGFZ), and Tehuantepec Ridge (TR). Four-letter station codes were shortened by dropping the -IG ending common to all of them.

based on the frequency of the noise affecting each record. The low frequency corner was chosen in the range from 0.01 to 0.04 Hz (periods between 100 and 25 s) while the high frequency corner varied between 1.0 and 1.5 Hz (from 1 to 0.67 s), which is appropriate for the phases used and the expected delay times (Wolfe and Silver, 1998). A time segment including only the selected phase was cut from the seismogram. In Figure 2 the time series is 33 s long and is typical of the record lengths used throughout this work. Figure 3 shows the combination of $(\phi, \delta t)$ producing the minimum eigenvalue, λ_2^{min}. The black dot means that the delay time, δt, is 1.05 s and the fast axis, ϕ, is 8° east of north. The first contour around the dot bounds the 95% confidence interval for the measurement. All the
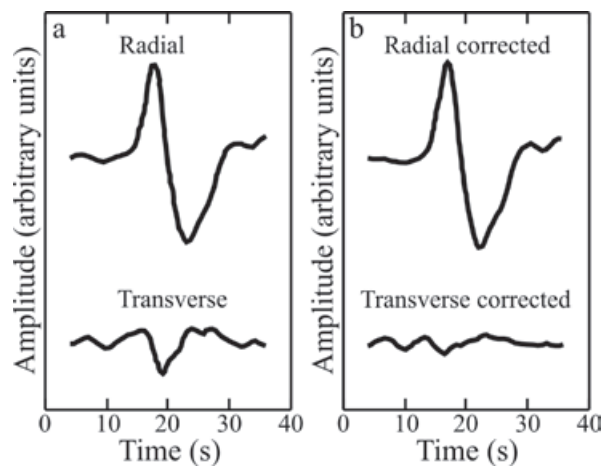
Figure 2. *SKS* wave from the event of May 16, 1998 south of the Fiji Islands (22.14°S, 179.70°W, h = 586 km, M = 5.9) recorded at broadband station Oaxaca (OXIG). The epicentral distance is 90.10°. (a) The radial and transverse velocity components are shown. (b) The radial and transverse components are shown after correcting for splitting using the values that were measured.

Table 1. Source parameters of the earthquakes used to measure upper mantle anisotropy.

| Date Y/M/D	Origin time H:M:S	Lat. (°N)	Long. (°E)	Depth (km)	Mag.	Location
1998/05/16	02:22:03	-22.14	-179.70	586	5.9	South of Fiji Islands
1998/08/20	06:40:52	28.97	139.40	400	6.2	Bonin Islands region
1998/11/08	07:25:49	-8.90	121.43	10	6.3	Flores region, Indonesia
1999/02/22	01:00:32	-21.52	169.66	10	6.4	Loyalty Islands region
1999/04/05	11:07:52	-5.31	149.84	10	7.4	New Britain region, Papua New Guinea
1999/04/08	13:10:34	43.60	130.53	560	7.2	Eastern Russia-northeastern China
1999/04/13	10:38:47	-21.38	-176.54	163	6.6	Fiji Islands region
1999/04/20	19:04:08	-31.83	-179.07	96	6.5	Kermadec Islands
1999/05/12	17:59:21	43.02	143.84	98	6.2	Hokkaido region, Japan
1999/05/17	10:07:59	-4.56	152.96	10	6.9	New Ireland region, Papua New Guinea
1999/07/07	18:52:57	49.25	155.54	10	6.2	Kuril Islands
1999/07/28	10:08:21	-30.24	-177.98	10	6.2	Kermadec Islands
1999/08/01	08:39:08	-30.44	-177.84	10	6.4	Kermadec Islands
1999/10/18	02:43:24	-56.00	-26.50	10	6.1	South Sandwich Islands region
1999/11/12	16:57:20	40.77	31.15	10	7.2	Turkey
1999/11/26	13:21:15	-16.45	168.18	10	7.1	Vanuatu Islands
2000/01/08	01:19:46	-9.93	160.05	10	6.4	Solomon Islands
2000/03/28	11:00:20	22.41	143.59	116	7.7	Volcano Islands region, Japan
2000/05/06	13:44:17	-11.26	165.41	10	6.3	Santa Cruz Islands
2000/06/06	14:57:02	29.47	131.41	10	6.0	Southeast of Ryukyu Islands
2000/06/14	02:15:25	-25.57	177.97	604	6.4	South of Fiji Islands
2000/08/15	04:30:09	-31.52	179.68	358	6.6	Kermadec Islands region
2000/08/21	09:16:25	-53.08	-46.32	10	6.1	South Atlantic Ocean
2000/08/28	19:29:26	-4.15	127.21	48	6.4	Banda Sea
2000/10/29	08:37:03	-5.18	154.00	100	6.3	Solomon Islands
2000/11/07	00:18:06	-55.25	-29.18	10	6.8	South Sandwich Islands region
2000/11/17	21:01:56	-5.49	151.66	10	7.5	New Britain region, Papua New Guinea
2001/01/26	03:16:41	23.40	70.32	24	7.9	Southern India
2002/04/26	16:06:06	13.11	144.56	85	7.1	Mariana Islands
2002/05/08	05:26:00	-17.94	-174.65	131	6.3	Tonga Islands
2002/06/06	23:53:51	-0.88	148.20	10	6.3	Admiralty Islands, Papua New Guinea
2002/06/22	02:58:20	35.63	48.95	10	6.5	Western Iran
2002/06/28	17:19:30	43.77	130.72	564	7.3	Eastern Russia-northeastern China
2002/08/02	23:11:39	29.32	139.04	425	6.2	Southeast of Honshu, Japan
2002/08/15	05:30:29	-1.25	121.36	10	6.2	Sulawesi, Indonesia
2002/08/19	11:01:01	-21.80	-179.49	587	7.6	Fiji Islands region
2002/09/08	18:44:26	-3.24	142.89	10	7.6	New Guinea, Papua New Guinea
2002/09/15	08:39:31	44.86	130.08	578	6.5	Northeastern China
2002/10/04	19:05:50	-20.82	-179.00	627	6.4	Fiji Islands region
2002/10/14	14:12:43	41.34	142.06	58	6.1	Hokkaido region, Japan
2002/10/22	11:39:04	-20.47	-178.62	552	6.2	Fiji Islands region
2003/01/20	08:43:06	-10.42	160.70	10	7.3	Solomon Islands
2003/02/10	04:49:30	-6.02	149.82	10	6.3	New Britain region, Papua New Guinea
2003/03/02	16:42:56	-36.80	-20.73	10	6.2	Southern Mid-Atlantic Ridge
2003/03/11	07:27:32	-4.70	153.13	10	6.8	New Ireland region, Papua New Guinea
2003/05/13	21:21:13	-17.40	167.66	10	6.2	Vanuatu Islands
2003/05/21	18:44:18	36.88	3.73	10	6.8	Northern Algeria
2003/06/12	08:59:20	-5.94	154.70	185	6.2	Bougainville region, Papua New Guinea
2003/08/04	04:37:20	-60.56	-43.49	10	7.5	Scotia Sea
2003/08/21	12:12:50	-45.18	167.12	10	7.0	South Island of New Zealand
2003/09/26	20:38:21	42.05	144.47	10	6.0	Hokkaido region, Japan
2003/09/29	02:36:54	42.44	144.39	10	6.5	Hokkaido region, Japan
2003/10/08	09:06:55	42.66	144.49	10	6.7	Hokkaido region, Japan
2003/10/18	22:27:13	0.52	126.05	10	6.4	Molucca Sea
2003/10/31	01:06:28	37.83	142.59	10	7.0	Honshu, Japan
2003/12/27	16:00:59	-22.03	169.65	10	7.3	Southeast of the Loyalty Islands
2004/01/03	16:23:18	-22.30	169.70	10	7.1	Southeast of the Loyalty Islands

Figure 3. Contour plot showing the minimum value in $(\phi, \delta t)$-space as indicated by the dot. In this case the fast polarization direction is N8°E and the delay time is 1.05 s. The first contour around the dot bounds the 95% confidence region.

other contours are multiples of the first one and are located at higher "elevations" or mountains. The black dot is located at the bottom of a valley. The 95% confidence contour was calculated using equation (16) in Silver and Chan (1991) and taking one degree of freedom for each second of the record containing the *SKS* arrival (Silver and Chan, 1991; K. M. Fischer, Brown University, personal communication, 1998). The uncertainties are read directly from the contour plots. In this case, the measurement with its $\pm 1\sigma$ uncertainty is $(\phi, \delta t) = (8\pm27°, 1.05\pm0.65$ s$)$. In the event that the 95% confidence region is not approximately symmetric, the largest of the two possible 1σ values is used, i. e. in going from 8° to 35°, as opposed to going from 8° to -5° (Figure 3). The contour plots are also useful to gauge the quality of the measurements. For example, a large 95% confidence area means that the parameters are poorly constrained. If multiple minima occur then the measurement is not reliable. Another possibility is that the 95% contour does not close, thus indicating a null measurement. All the individual splitting measurements are reported in Table 2.

It is important to run a number of checks in order to make sure that the observation of *SKS* energy on the transverse component is indeed the result of anisotropy and does not arise from a different process such as scattering (Silver and Chan, 1991; Savage, 1999). Likewise, these checks mean that the values determined for ϕ and δt are reliable. (1) An "unsplitting" correction is applied to the radial and transverse records using the estimated splitting parameters. If $(\phi, \delta t)$ do describe anisotropy, then the *SKS* wave must disappear, or at least its amplitude is decreased, from the corrected transverse component (Figure 2b). Similarly, the amplitude of *SKS* is increased on the corrected radial component, although this effect is small. (2) The particle motion of the *SKS* arrival in the transverse component is plotted as function of the radial component. Before the unsplitting correction, particle motion must be approximately elliptical (Figure 4a), and after correction it becomes nearly linear (Figure 4b). (3) The N-S and E-W records are rotated through the

Figure 4. A further check was a comparison of the particle motion in the transverse component as a function of the radial. (a) Before correcting for the anisotropy the particle motion is elliptical. (b) After a correction for the measured anisotropy is applied, the particle motion becomes close to linear.
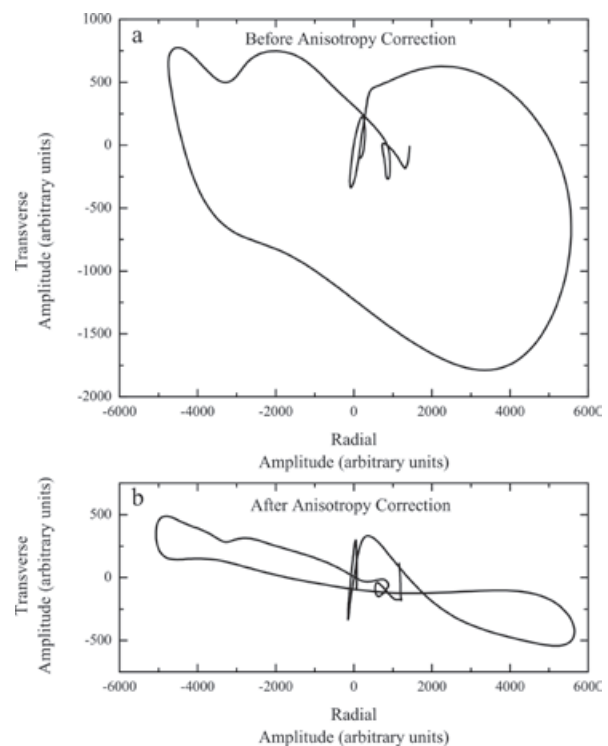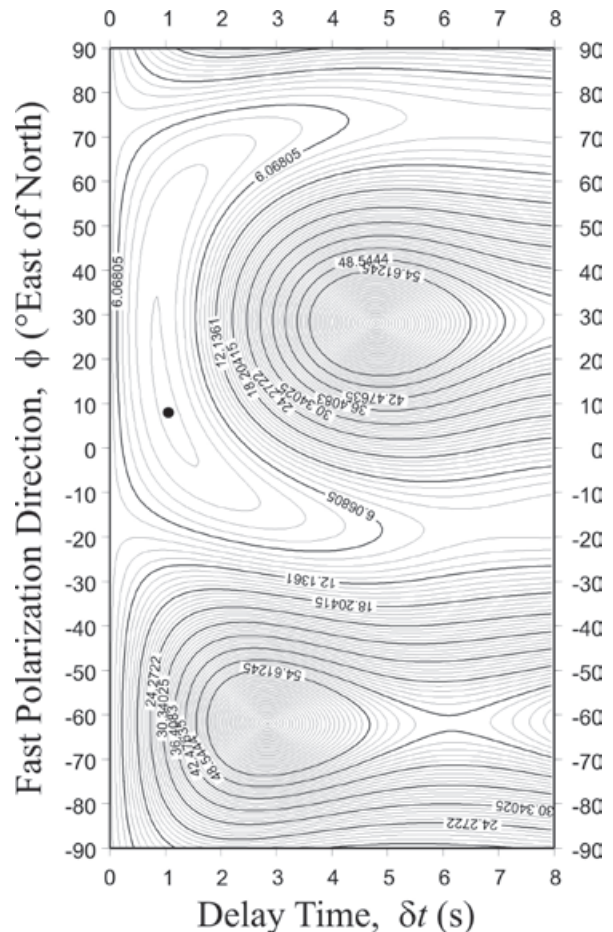
Table 2. Individual splitting parameters measured at each station.

Station	Date Y/M/D	φ_b (°)	Phase	φ (°)	σ_φ (°)	δt (s)	$\sigma_{\delta t}$ (s)
CAIG	2000/03/28	300.22	SKS	-84	51	0.95	0.85
	2000/03/28	300.22	sSKS	37	38	2.25	1.65
	2002/06/28	324.69	SKS	42	77	1.10	1.60
	2003/05/13	254.08	SKS	50	31	1.60	0.90
	2003/10/31	314.47	SKS	42	-	-	-
CCIG	2002/06/28	328.76	SKS	-13	66	0.50	4.20
	2003/05/13	255.90	SKS	48	45	0.80	1.00
	2003/09/29	320.97	SKS	-19	55	0.70	1.90
CJIG	1998/05/16	244.16	SKS	-31	-	-	-
	2000/08/21	148.88	SKS	-23	12	1.35	0.55
	2002/06/28	322.76	SKS	-17	11	0.55	0.30
	2002/08/19	244.39	SKS	-31	-	-	-
	2002/10/04	245.10	SKS	-41	-	-	-
CMIG	2002/04/26	293.39	sSKS	20	-	-	-
	2002/06/22	32.68	SKKS	44	-	-	-
	2002/10/04	248.63	SKS	54	5	1.70	0.50
	2002/10/22	248.86	SKS	52	-	-	-
	2003/05/13	255.45	SKS	50	60	1.00	0.90
	2003/08/04	157.23	SKS	67	-	-	-
	2003/08/21	227.36	SKS	54	-	-	-
	2003/10/31	316.79	SKS	51	-	-	-
COIG	1999/04/05	270.48	SKS	24	38	0.80	1.00
	2000/03/28	299.22	SKS	18	-	-	-
	2000/05/06	259.82	SKS	48	59	1.15	1.15
	2002/10/14	316.57	SKS	-30	42	1.10	0.60
	2003/05/13	253.32	SKS	17	41	0.60	0.90
	2003/05/21	49.85	SKS	44	-	-	-
	2003/06/12	268.28	SKS	72	64	0.85	0.95
CUIG	2000/05/06	261.25	SKS	38	55	1.20	1.25
HUIG	1999/02/22	250.44	SKS	59	-	-	-
	1999/04/13	247.08	SKS	65	-	-	-
	1999/07/07	321.63	SKS	51	-	-	-
	1999/07/28	239.08	SKS	63	-	-	-
	1999/08/01	238.85	SKS	63	-	-	-
	1999/11/26	255.74	SKS	66	-	-	-
	2000/05/06	261.50	SKS	50	43	1.10	0.60
	2000/06/14	244.58	SKS	63	-	-	-
	2002/10/04	248.31	SKS	66	-	-	-
	2002/10/22	248.54	SKS	59	-	-	-
	2003/05/13	254.93	SKS	66	-	-	-
LVIG	1998/05/16	247.19	SKS	43	11	1.15	0.55
	2003/05/13	255.57	SKS	44	56	1.45	1.75
	2003/12/27	250.52	SKS	46	65	1.60	2.60
	2004/01/03	250.24	SKS	47	12	1.40	0.70

Table 2. Continuation.

Station	Date Y/M/D	φ_b (°)	Phase	φ (°)	σ_φ (°)	δt (s)	$\sigma_{\delta t}$ (s)
MOIG	2000/08/15	237.13	SKS	-60	47	0.90	0.80
	2002/06/22	27.29	SKKS	55	26	0.95	0.35
	2002/08/15	288.85	PKS	25	-	-	-
	2002/08/19	245.80	SKS	-85	50	0.45	1.25
	2002/09/15	325.72	SKS	77	18	1.35	0.55
	2002/09/15	325.72	SKKS	51	-	-	-
	2003/10/08	317.76	SKS	89	-	-	-
OXIG	1998/05/16	247.05	SKS	8	27	1.05	0.65
	1999/04/08	326.42	SKS	42	30	1.20	0.70
	1999/04/20	237.71	SKS	49	13	1.35	0.45
	1999/05/12	319.87	SKS	38	60	1.75	1.65
	1999/10/18	147.96	SKS	35	22	1.20	0.40
	2000/03/28	301.82	SKS	32	-	-	-
	2000/08/28	281.77	PKS	7	-	-	-
	2002/08/02	310.28	SKS	32	7	2.15	0.65
	2002/09/08	276.40	SKS	28	55	1.15	1.55
	2002/09/15	327.60	SKS	11	33	0.65	0.40
	2002/10/04	248.09	SKS	41	23	0.85	0.45
	2003/05/13	254.99	SKS	41	26	1.35	0.55
	2003/10/08	319.30	SKS	35	23	1.25	1.20
PLIG	1999/04/08	325.21	SKS	70	10	2.00	1.00
	1999/05/17	271.32	SKS	38	19	1.70	0.30
	1999/10/18	147.24	SKS	-18	68	1.05	0.55
	1999/11/12	36.62	SKS	70	38	1.25	0.75
	2000/03/28	300.90	SKS	58	34	0.95	0.75
	2000/03/28	300.90	sSKS	34	14	2.15	1.15
	2000/05/06	261.01	SKS	13	10	1.35	0.45
	2000/06/06	313.39	SKS	51	-	-	-
	2000/06/14	243.71	SKS	32	46	0.65	0.85
	2000/08/15	237.62	SKS	46	56	1.00	1.20
	2002/04/26	291.79	sSKS	42	65	0.70	0.80
	2002/06/28	325.24	SKS	73	7	1.85	0.65
	2002/08/02	309.22	SKS	54	86	0.80	1.20
	2002/08/19	246.43	SKS	52	18	0.95	0.55
	2002/09/08	276.11	SKS	5	-	-	-
	2002/09/15	326.39	SKS	73	8	2.05	1.05
	2002/10/04	247.18	SKS	23	30	0.70	0.50
	2003/01/20	263.19	SKS	67	13	1.85	0.85
	2003/02/10	270.86	SKS	16	50	1.55	0.75
	2003/05/13	254.46	SKS	19	23	1.05	0.35
	2003/08/21	227.12	SKS	50	-	-	-
	2003/10/18	287.97	PKS	40	20	1.50	0.70
PNIG	1998/08/20	308.92	SKS	20	-	-	-
	1999/10/18	147.65	SKS	23	73	0.45	2.55
	2000/03/28	300.98	SKS	16	-	-	-
	2000/03/28	300.98	sSKS	14	-	-	-
	2002/06/28	325.63	SKS	26	51	0.50	0.40
	2002/09/15	326.79	SKS	18	58	0.60	2.20
PPIG	2000/01/08	264.29	SKS	31	51	1.40	1.55
	2001/01/26	14.73	PKS	32	9	2.15	0.75
	2002/09/08	276.79	SKS	24	14	2.15	0.85
	2003/08/04	156.03	SKS	22	56	1.80	2.55

Table 2. Continuation.

Station	Date Y/M/D	φ_b (°)	Phase	φ (°)	σ_φ (°)	δt (s)	$\sigma_{\delta t}$ (s)
SCIG	2002/05/08	251.16	SKS	-16	-	-	-
	2003/03/02	130.64	SKS	-49	-	-	-
TEIG	1998/05/16	249.78	SKS	61	19	1.40	0.90
	1999/04/08	331.62	SKS	59	-	-	-
	1999/05/12	323.97	SKS	67	-	-	-
	2002/06/28	331.62	SKS	60	-	-	-
	2003/08/04	159.58	SKS	70	-	-	-
TPIG	2003/03/11	271.81	SKS	35	13	1.50	0.30
	2003/06/12	270.07	SKS	32	21	1.45	0.55
	2003/08/21	227.39	SKS	44	-	-	-
TUIG	1998/05/16	247.75	SKS	53	49	1.25	1.25
	1999/05/12	320.91	SKS	52	-	-	-
	1999/10/18	148.51	SKS	66	-	-	-
	2002/08/02	311.75	SKS	44	-	-	-
YAIG	1998/05/16	246.31	SKS	55	66	0.40	1.20
	1999/11/12	36.77	SKS	61	22	1.40	0.70
	2000/03/28	301.22	SKS	56	14	2.15	0.85
	2000/03/28	301.22	sSKS	70	24	1.05	0.55
	2000/08/15	237.77	SKS	70	-	-	-
	2002/06/28	325.52	SKS	82	-	-	-
	2002/09/15	326.66	SKS	78	-	-	-
	2003/01/20	263.43	SKS	89	-	-	-
	2003/09/26	318.17	SKS	74	-	-	-
	2003/09/29	318.38	SKS	70	33	1.60	1.25
	2003/10/31	315.19	SKS	52	-	-	-
ZAIG	1998/11/08	281.19	PKS	-78	-	-	-
	1999/05/17	271.54	SKS	-87	-	-	-
	1999/10/18	146.14	SKS	-57	27	1.05	0.45
	2000/06/14	242.75	SKS	-62	28	0.90	0.40
	2000/08/15	236.74	SKS	-64	28	0.75	0.35
	2000/10/29	270.55	SKS	-88	-	-	-
	2000/11/07	146.11	SKS	-89	38	1.00	1.00
	2000/11/17	271.17	SKS	-78	-	-	-
	2002/06/06	276.99	SKS	-80	-	-	-
	2002/08/19	245.14	SKS	-60	16	0.85	0.20
	2002/10/14	317.17	SKS	-56	40	1.10	1.00
ZIIG	1999/04/08	324.15	SKS	-16	37	0.55	0.35
	1999/04/08	324.15	SKKS	-29	92	1.45	2.05
	2002/06/28	324.19	SKS	-8	32	0.50	0.35
	2002/09/15	325.35	SKKS	-14	71	1.20	1.75

Dates of the earthquakes and the phases used to measure individual splitting parameters at each station. φ_b is the back azimuth. Parameter φ is the fast polarization direction (measured east of north), δt is the delay time, and σ_φ and $\sigma_{\delta t}$ are the 1σ uncertainties.
Null measurements are represented with a nonzero value for φ and dashes for the next three columns. Therefore, any of the three following situations could occur for the particular earthquake-to-station path being considered: $\varphi \approx \varphi_b$, $\varphi \approx \varphi_b \pm 90°$, or $\delta t \approx 0$ s. The actual value listed for φ is used as a possible interpretation of the data and is intended as additional information where appropriate.

angle ϕ to obtain the slow and fast components of the *SKS* pulse. The fast and slow waveforms must have roughly the same shape and the fast *SKS* must arrive before the slow *SKS* by an amount approximately equal to the measured δt (Figure 5). Shifting the slow wave forward by a time δt should align it with the fast wave.
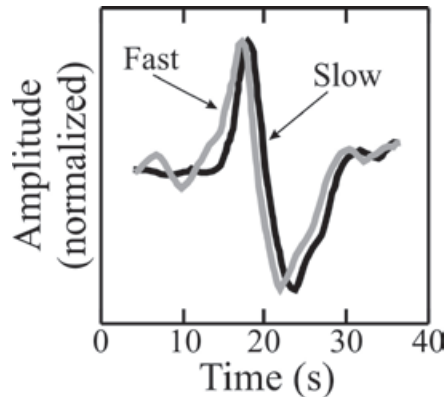

Figure 5. Once the fast polarization direction is known, the N-S and E-W horizontal records are rotated through the angle ϕ in order to obtain the slow and fast components of the *SKS* pulse. These are shown normalized to the same amplitude.

Results

Table 1 lists the events that provided useful data for this study. Earthquake information includes the date, origin time, hypocenter, magnitude, and the geographic location. A total of 136 individual splitting measurements were made at twenty different stations and are given in Table 2. The parameters are the fast polarization direction and the delay time, both with their corresponding 1σ uncertainties. Also provided are the date of the event, the back azimuth, and the phase used (*SKS, SKKS, sSKS,* or *PKS*). The observed orientations of the fast polarization direction practically span the whole space of possible solutions, from -90 to 90°. The smallest $1\sigma_\phi$ uncertainty for the fast polarization direction is 5°, while the largest is 92°. The latter value is quite large and such an estimate normally would not be reliable. In general, such large uncertainties arise from a poor signal-to-noise ratio. We allowed large uncertainties for a few measurements if the data at the station were scarce. Furthermore, Wolfe and Silver (1998) showed that in certain cases, stacking measurements with large error regions can lead to improved estimates of the splitting parameters. As explained below, our measurements for each station were averaged using the stacking method proposed by Wolfe and Silver (1998) and consequently have smaller 1σ uncertainties than the individual measurements. It

is worth mentioning that the average uncertainty in Table 2 is 37°. The smallest delay time is 0.40 s and the largest is 2.25 s. The average delay time is 1.20 s. The smallest $1\sigma_{\delta t}$ uncertainty for the delay time is 0.20 s, and the largest is 4.20 s at station CCIG, although this is an extreme value. The second largest $1\sigma_{\delta t}$ uncertainty is 2.60 s. The average uncertainty, however, is much lower at 0.96 s. The station with the largest number of observations is PLIG with nineteen records showing clearly split waveforms and three null measurements given that it had the largest number of records meeting the selection criteria previously explained. Station CUIG had the fewest observations, only one with a clearly split waveform was available. Since this station is located within Mexico City, cultural noise is certainly a problem. On average, 6.8 measurements are reported per station. Some sites are noisier than others. Additionally, the stations were not installed simultaneously and some of them had been running for only a short time when the data for this study were gathered. Even though records from 359 different earthquakes were analyzed, only 57 of them generated observable *P* to *S* CMB conversions at the various stations. The individual splitting parameters are shown in Figure 6.

Average splitting parameters were calculated for each station using the stacking method of Wolfe and Silver (1998). The error surface associated to the contour plot of each individual measurement is normalized by its minimum eigenvalue, $\lambda_{2,i}^{min}$. The normalized error surfaces from all measurements at the station are then summed. In this way, the best splitting parameters are given by the minimum value of the sum and a new 95% confidence interval is obtained. As the noise properties vary for different earthquakes, stacking events with a similar polarization improves the final result (Wolfe and Silver, 1998). Therefore, the size of the 95% confidence region for the averaged values is smaller than for the individual measurements. The averaged splitting parameters are presented in Table 3, which includes the fast polarization direction and the delay time, both with their corresponding 1σ uncertainties, as well as the stations' coordinates and geographic location, and the total number of clearly split and null measurements. In this case, the smallest $1\sigma_\phi$ uncertainty for the fast polarization direction is 4°, while the largest is 21°. Strictly speaking, there are three uncertainties of 55, 43, and 49° at stations CUIG, HUIG, and TUIG, respectively. These stations only had one split measurement each and so the individual measurement is reported as the average. As shown in Table 2 and in Figure 6, the results at stations HUIG and TUIG are considered reliable because they also had null measurements consistent with the only split value reported. The average $1\sigma_\phi$ uncertainty in Table 3 is 16°. The smallest delay time is 0.50 s and the
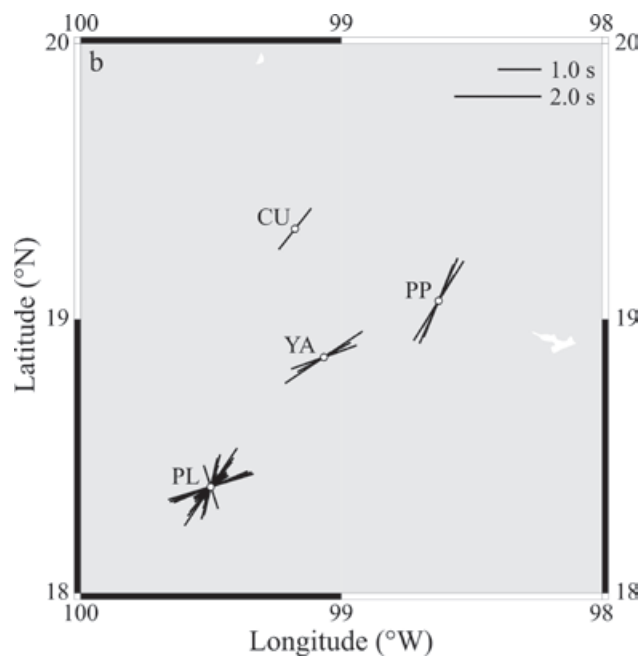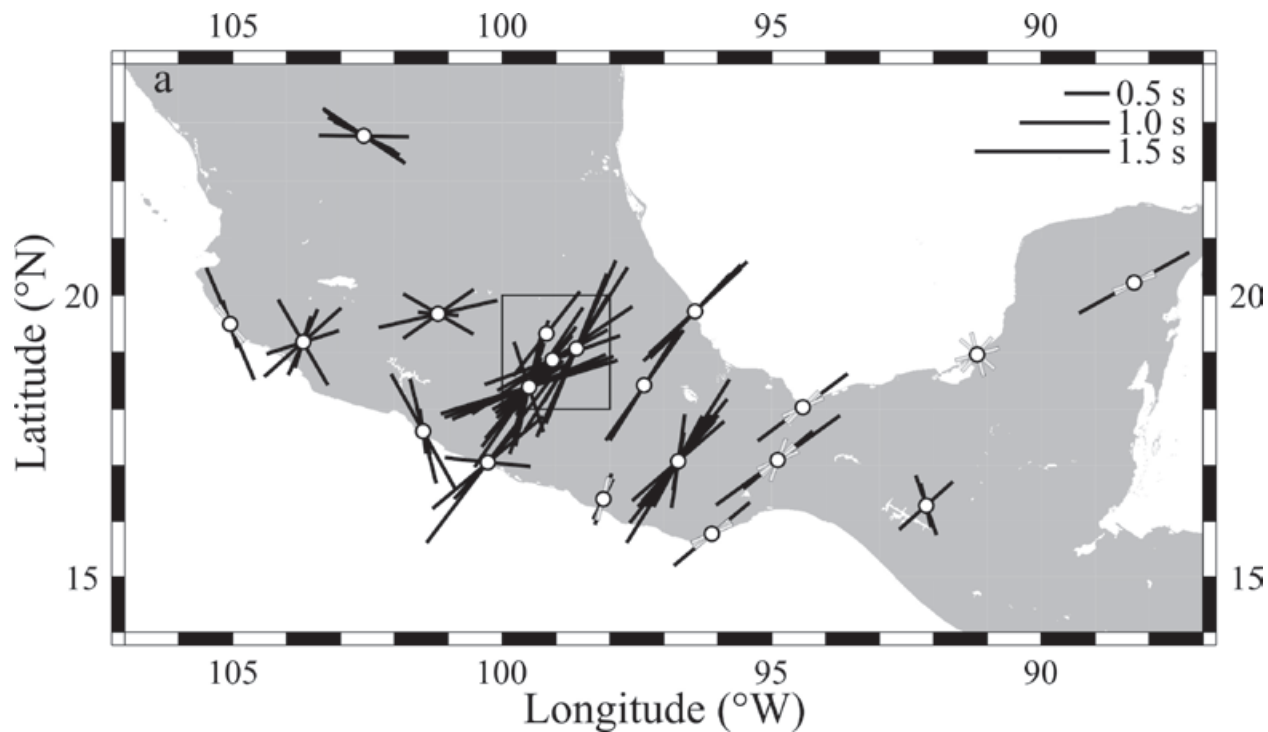
Figure 6. (a) Individual measurements of ϕ and δt at stations in southern Mexico. Symbols are as in Figure 1. Additionally, null measurements from two nonorthogonal back azimuths are represented by the white bars (forming two crosses) for station SCIG, which is interpreted to have splitting below the threshold of the data. Other null measurements are shown only for stations with a few well constrained splitting measurements. The fast directions for these null measurements were chosen to be consistent with the split observations. The box represents the area shown as an inset in (b).

largest is 1.90 s. The average delay time is 1.09 s. The smallest $1\sigma_{\delta t}$ uncertainty for the delay time is 0.10 s, while the largest is 1.25 s. The average uncertainty is 0.46 s. Station SCIG only had two null measurements from nonorthogonal back azimuths, so it is interpreted to have splitting below the threshold of the data. The averaged splitting parameters are shown in Figure 1.

Discussion

Figure 1 shows the averaged splitting parameters at each station and the tectonic environment of the study area. The best coverage is found between 94 and 101°W longitude. The study area was divided into several regions based on variations in the tectonic environment as well as differences in the measured anisotropy parameters. They are discussed below.

Mexican Subduction Zone Between 96 and 101°W Longitude

In this region (Figure 1), subduction of the Cocos plate under the North American plate at the Middle America Trench (MAT) is bounded by the landward extension of the Orozco Fracture Zone (OFZ) and the Tehuantepec Ridge (TR). The relative velocity between the Cocos and North American plates increases from 5.7 cm/yr in the northwest to 7.3 cm/yr in the southeast (model PVEL in DeMets *et al.* (2010)) while the Cocos plate moves in the direction ~N31°E. The fast polarization direction for many stations in this region is approximately the same as the relative

Table 3. Averaged splitting parameters measured at each station.

Station	Lat. (°N)	Long. (°E)	φ (°)	σ_φ (°)	δt (s)	$\sigma_{\delta t}$ (s)	N Split	Null	Location
CAIG	17.05	-100.27	43	10	1.30	0.60	4	1	El Cayaco, Gro.
CCIG	16.28	-92.14	18	18	0.60	0.25	3	0	Comitán, Chis.
CJIG	19.50	-105.04	-18	13	0.70	0.40	2	3	Chamela, Jal.
CMIG	17.09	-94.88	53	10	1.60	0.50	2	6	Col. Cuauhtémoc, Oax.
COIG	19.18	-103.69	17	21	0.75	0.40	5	2	Colima, Col.
CUIG[a]	19.33	-99.18	38	55	1.20	1.25	1	0	Ciudad Universitaria, D. F.
HUIG	15.77	-96.11	50	43	1.10	0.60	1	10	Huatulco, Oax.
LVIG	19.72	-96.42	45	7	1.35	0.45	4	0	Laguna Verde, Ver.
MOIG	19.68	-101.19	71	5	1.00	0.20	4	3	Morelia, Mich.
OXIG	17.08	-96.72	28	6	0.90	0.20	11	2	Oaxaca, Oax.
PLIG	18.39	-99.50	57	5	1.10	0.20	19	3	Platanillo, Gro.
PNIG	16.40	-98.13	23	11	0.50	0.30	3	3	Pinotepa Nacional, Oax.
PPIG	19.07	-98.63	34	6	1.90	0.35	4	0	Popocatépetl, Tlamacas, Pue.
SCIG	18.97	-91.19	00	-	-	-	0	2	Sabancuy, Camp.
TEIG	20.23	-88.28	61	19	1.40	0.90	1	4	Tepich, Q. R.
TPIG	18.42	-97.36	32	13	1.50	0.40	2	1	Tehuacán, Pue.
TUIG	18.03	-94.42	53	49	1.25	1.25	1	3	Tuzandépetl, Ver.
YAIG	18.86	-99.07	70	4	1.15	0.15	5	6	Yautepec, Mor.
ZAIG	22.77	-102.57	-61	5	0.85	0.10	6	5	Zacatecas, Zac.
ZIIG	17.61	-101.47	-13	13	0.60	0.20	4	0	Zihuatanejo, Gro.

Parameter φ is the fast polarization direction (measured east of north), δt is the delay time, and σ_φ and $\sigma_{\delta t}$ are the 1σ uncertainties. Averages were calculated using the stacking method of Wolfe and Silver (1998). N is the number of measurements available for analysis. The abbreviations after the locations stand for the names of Mexican states.
The station with a 00 value for φ and dashes for the next three columns does not exhibit splitting from at least two different nonorthogonal back azimuths (φ_b) and is interpreted as having splitting below the threshold of the data.
[a]Data at station CUIG are noisy, a measurement is provided but it is poorly constrained.

plate motion (RPM) between the Cocos and North American plates, and approximately perpendicular to the MAT. Most of these stations overlie the Cocos plate where it subducts subhorizontally (Pardo and Suárez, 1995; Pérez-Campos *et al.,* 2008; Husker and Davis, 2009) and likely reflect the flow direction of the upper mantle below the slab. Given the conditions expected to prevail beneath the slab, such as low stress, low water content, and relatively high temperature, we assume that the lattice preferred orientation (LPO) of olivine is of type-A (Jung *et al.,* 2006; Long and Silver, 2008). Therefore, the fast anisotropy axis and mantle flow are oriented in the same direction. It also follows that flow is entrained under the subhorizontal Cocos slab. Most regions

with substantial subslab splitting around the world, however, show trench-parallel ϕ, which is interpreted as 3-D return flow induced by trench migration (Long and Silver, 2008). Perhaps the most notable exception is the Cascadia subduction zone, where a trench-perpendicular pattern has been found (Currie *et al.,* 2004; Long and Silver, 2008). Trench-perpendicular fast directions have also been reported by other studies in Mexico using *SKS* phases. Soto *et al.* (2009) found trench-perpendicular ϕ where the Rivera plate subducts beneath the Jalisco block (the region between stations CJIG and COIG in Figures 1 and 7 of this study). Data from the Mesoamerican Subduction Experiment (MASE) array, a line of 100 seismometers running north and starting just east
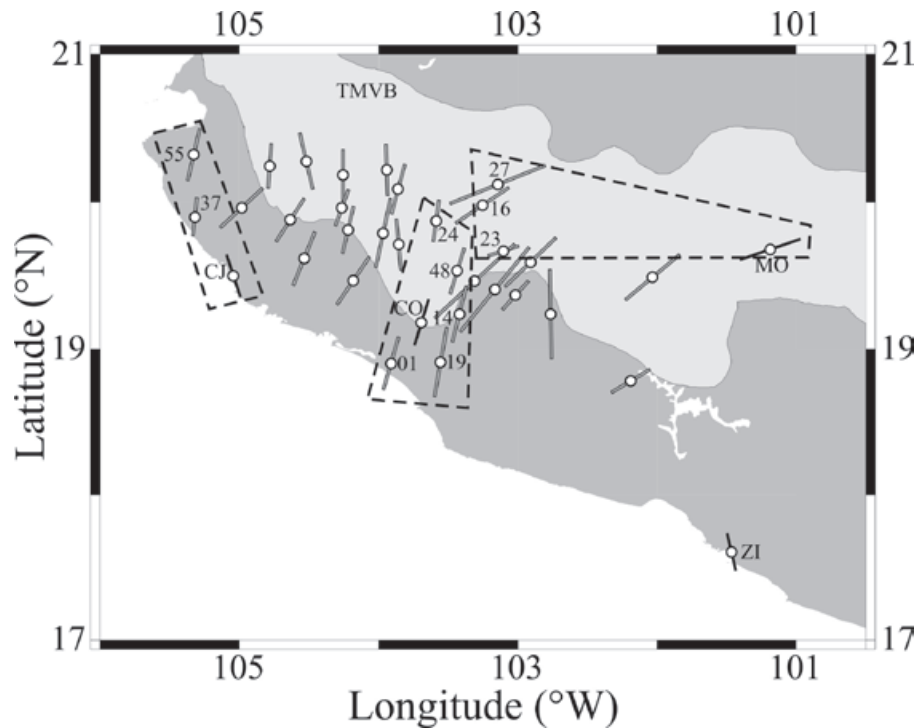
Figure 7. Map showing the relationship between measurements made at the MARS stations (Soto *et al.,* 2009) and those from SSN stations in the present study. The stations enclosed by dashed-line polygons are discussed in the main text. MARS station codes were shortened by dropping the MA- prefix.

of CAIG (Figure 1), show an average ϕ of N41°E for stations in the fore-arc, while ϕ averages N8°W for stations in the back-arc (the volcanic arc is located at the southern edge of the Trans-Mexican Volcanic Belt) (Stubailo and Davis, 2007, 2012a, 2012b; Rojo-Garibaldi, 2012). Farther east, measurements from the Veracruz-Oaxaca (VEOX) profile, a line of 46 seismometers running north-south across the Isthmus of Tehuantepec (just west of CMIG in Figure 1), reveal fast directions consistent with nearby SSN stations TUIG, CMIG, and HUIG (Bernal-Díaz *et al.,* 2008).

In order to allow for the 3-D return flow induced by trench migration observed at most subduction zones, Long and Silver (2008, 2009) propose the existence of a thin decoupling zone between the downgoing slab and the subslab mantle. The decoupling zone may result from the entrainment of a thin layer of buoyant asthenosphere which is produced through shear strain and shear heating (Phipps Morgan *et al.,* 2007; Long and Silver, 2008, 2009). In this study, however, the approximately trench-perpendicular fast directions observed beneath the Cocos plate in the Mexican states of Guerrero and Oaxaca, just like observations at Cascadia (Long and Silver, 2009), suggest that the thin decoupling zone does not exist. Therefore, the downgoing slab and sub-slab mantle are coupled at depth, which results in entrained flow. The age of the subducting oceanic Cocos plate at the MAT offshore Guerrero and Oaxaca is approximately between 12 and 16 Myr

(Kanjorski, 2003). Both Cascadia and the Middle America Trench represent the most extreme examples of the subduction of young lithosphere. Consequently, Long and Silver (2009) hypothesize that the amount of strain is not yet high enough for the shear mechanism to reach steady state and so decoupling has not yet occurred. Farther east along the MAT, in Nicaragua and Costa Rica, Abt *et al.* (2010) interpret their anisotropy measurements using teleseismic *SKS* and local *S* phases as mantle flow parallel to the trench, both beneath the subducted Cocos slab and in the mantle wedge. The age of the lithosphere subducting at the MAT there is between 18 and 24 Myr (Abt *et al.,* 2009).

The trench-perpendicular fast directions found beneath the Cocos plate in Guerrero and Oaxaca in the present study stand in contrast to the trench-parallel fast directions observed by Stubailo *et al.* (2012) using Rayleigh waves. They obtained phase velocity maps for waves of different periods in the range from 16 to 100 s. Since phase velocities provide a depth-integrated image of the upper mantle, they inverted the phase velocity maps and determined a 3-D model for shear wave velocity and anisotropy. Their model is parameterized into three layers: the continental crust, mantle lithosphere, and asthenosphere down to a depth of 200 km. Both the lithospheric and asthenospheric layers show trench-parallel fast directions in the fore-arc with values ranging between 0.5 and 2% ψ in anisotropy. Farther west, coincident with

the landward projection of the Orozco Fracture Zone, the fast axes become trench-perpendicular. Stubailo *et al.* (2012) interpret these results as toroidal flow into the mantle wedge coming in from the two edges that limit the segment of the Cocos slab located between the OFZ to the east and the Rivera slab to the west. If the trench-parallel fast directions observed by Stubailo *et al.* (2012) in Guerrero and Oaxaca, where the slab is subhorizontal, are interpreted as 3-D return flow produced by trench rollback, this would be inconsistent with our interpretation of entrained flow. The delay times measured from *SKS* splitting in this region range from 0.5 to 1.9 s. Using the common assumption that shear wave anisotropy is 4% (Silver and Chan, 1991; Savage, 1999), a delay time of 1 s corresponds to an effective thickness for the anisotropic layer of 115 km. Therefore, the observed delay times translate into anisotropic layer thicknesses between 60 and 220 km. It is possible that the anisotropic regions sampled by the Rayleigh and *SKS* waves are different given that their paths are different. The sensitivity kernel for a period of 100 s peaks at a depth of 140 km (Stubailo *et al.*, 2012) and so Rayleigh waves sample the lithosphere preferentially. Thus, if the *SKS* anisotropic layer is placed under the Rayleigh wave anisotropic layer, it would start at a depth of ~150 km. Admittedly, the vertical resolution for shear wave splitting is poor, but it is generally agreed that anisotropy resides in the shallow part of the upper mantle (Silver, 1996; Savage, 1999). If the anisotropic layer in the present study is placed too deep, however, it will no longer be in contact with the subducted slab and consequently entrained flow cannot be used to explain the observed anisotropy. A possible way to resolve this discrepancy may be to carry out a joint inversion of the surface wave and *SKS* data. Anisotropy in this region has also been reported by other researchers. Song and Kim (2012b) found that the upper oceanic crust of the subducting Cocos slab is an ultraslow-velocity layer (USL). It is 3 to 5 km thick and it shows anisotropy larger than 5%. Additionally, Song and Kim (2012a) discovered that the topmost 2-6 km of the Cocos subducted oceanic mantle is an anisotropic high-velocity lid (HVL).

The average $\delta t \pm \sigma_{\delta t}$ for stations in the fore-arc with trench-perpendicular ϕ is 1.20±0.41 s. The trench migration (retreating) velocity for this segment of the MAT is 21 mm/yr (Heuret and Lallemand, 2005). Long and Silver (2008) proposed a relationship for average subslab δt as a function of trench migration velocity, mostly for trench-parallel ϕ (Cascadia is an exception but it is also included). The values given above plot in their Figure 2 close to the entry for the MAT in Nicaragua and Costa Rica but δt is smaller for Guerrero and Oaxaca, so they are roughly consistent with the trend observed by Long and

Silver (2008). Calculation with the equation given in the caption to their Figure 2 predicts $\delta t = 0.72$ s for the MAT in Guerrero and Oaxaca.

Mexican Subduction Zone East of 96°W Longitude

A slight (~25°) clockwise rotation of the anisotropy fast axes is observed for stations HUIG, CMIG, and TUIG relative to nearby stations PNIG, OXIG, and TPIG which are located to the west (Figure 1). These directions are also consistent with preliminary *SKS* results from the N-S VEOX profile deployed just west of CMIG (Bernal-Díaz *et al.*, 2008). Using VEOX data and local earthquakes within the Cocos slab, León-Soto *et al.* (2011) found that the fast anisotropy axis is trench-perpendicular in the mantle wedge. Several changes in subduction zone morphology take place in this area: (1) The Middle America Trench makes a bend southeast of station HUIG. (2) The Tehuantepec Ridge intersects the MAT. The TR has long been recognized as a sharp contrast in the properties of the Cocos plate. The oceanic crust of the Guatemala Basin in the southeast is older and deeper than the region northwest of the TR; see Manea *et al.* (2005) for a review. (3) The coastline is farther away from the MAT than in the area located to the west, which implies the existence of a broad continental shelf. (4) The subducting Cocos plate is not subhorizontal anymore and dips at an angle of ~25° (Pardo and Suárez, 1995; Rodríguez-Pérez, 2007; Melgar and Pérez-Campos, 2011; Kim *et al.*, 2011). Furthermore, recent results suggest the possibility of a tear in the slab somewhere in the region where it changes from subhorizontal to a dip of ~25° (Pérez-Campos *et al.*, 2012). The rotation of the *SKS* fast axes may be caused by the change in dip of the Cocos slab. Furthermore, this orientation may be transitional to the orientation of the fast axis at station TEIG in the Yucatán peninsula, which coincides with the absolute motion of the North American plate.

Farther east (Figure 1), the fast axis is oriented NNE-SSW and has a short delay time (0.60±0.25 s) at station CCIG. This direction agrees with the RPM between Cocos and North America and is roughly trench-perpendicular. South of CCIG the hypocenters reach depths of ~175 km and the Cocos slab subducts more steeply (~45°) than in the region to the west (Rodríguez-Pérez, 2007). The fast direction may be consistent with corner flow within the mantle wedge.

Mexican Subduction Zone West of 101°W Longitude

A few stations are available at the western end of the subducting Cocos plate and around the Rivera plate. Between the MAT and the coastline, the

boundary between the Cocos and Rivera plates is continued by the bathymetric feature known as El Gordo Graben, which further extends on land as the N-S trending Colima rift. Additionally, Colima volcano is located within the rift. The Rivera plate subducts more steeply than the adjacent Cocos slab (Pardo and Suárez, 1995) and a gap between the two was imaged tomographically at depths greater than 150 km (Yang *et al.*, 2009). This gap is located under the rift. Delay times at stations CJIG, COIG, and ZIIG are short and range from 0.60 to 0.75 s (Figure 1). Soto *et al.* (2009) previously used data from CJIG and COIG together with records from the Mapping the Rivera Subduction Zone (MARS) experiment. The present study concurs with the interpretation of Soto *et al.* (2009). The fast direction at station CJIG, and also at their stations MA37 and MA55, shows that the subslab mantle beneath the fore-arc flows around the western edge of the Rivera slab as the subducted plate rolled back (Figure 7). The fast directions at COIG and stations MA01, MA14, MA19, MA24, and MA48 (Soto *et al.,* 2009) within the Colima rift (Figure 7) are consistent with mantle flow through the slab gap between the Rivera and Cocos plates, and perhaps with the fact that Colima volcano is located within the rift (Yang *et al.*, 2009). Ferrari *et al.* (2001) documented rollback of the Rivera plate based on the trenchward migration of the volcanic front and further proposed asthenospheric infiltration into the mantle wedge from both the western and eastern edges of the subducted Rivera slab. Recent results of laboratory, analog models of the Rivera and Cocos slabs reveal complex patterns of toroidal and corner flows in agreement with seismic anisotropy studies (Neumann *et al.,* 2012).

The *SKS* fast axis at station ZIIG is oriented N13°W and looks clearly different from observations to the east, where the fast axis is roughly parallel to the RPM between Cocos and North America (Figure 1). ZIIG is located near the projected extension of the Orozco Fracture Zone beneath the North American plate. The subducting Cocos plate dips more steeply west of the projected OFZ than to the east, where the subhorizontal slab is found (Pardo and Suárez, 1995). Both Stubailo *et al.* (2012) and Dougherty *et al.* (2012) presented evidence for a tear in the Cocos slab underneath the projection of the OFZ. The *SKS* anisotropy pattern at ZIIG is consistent with flow through the gap in between the two segments of the torn slab. Furthermore, Stubailo *et al.* (2012) interpreted the anisotropy in their Rayleigh wave data in terms of toroidal mantle flow around the slab edges driven by slab rollback (Ferrari, 2004). The fast anisotropy axes in the region around ZIIG from surface wave data sampling the mantle lithosphere and asthenosphere are oriented slightly east of north (Stubailo *et al.,* 2012) and

are somewhat different from the *SKS* data in the present study given that the fast axis at ZIIG is oriented slightly west of north.

Fast Axes Oriented With the Absolute Plate Motion of North America

The absolute motion of the North American plate throughout southern Mexico is about 4 cm/yr and is oriented in a direction ~N254°E according to model HS3-NUVEL1A in Gripp and Gordon (2002); see Figure 1. A few stations (MOIG, YAIG, and PLIG) in or near the TMVB have their fast directions aligned with the APM and their delay times range from 1.00 to 1.15 s. Such a pattern can be explained as the rigid lithosphere moves and consequently drags the asthenosphere below (Silver, 1996). It is expected in regions where other tectonic processes have not operated and is observed frequently. The alignment of the fast axes with the APM at these stations may signal a change in the tectonic regime as one moves away from the MAT. Soto *et al.* (2009) found the fast axes for stations within the Colima rift oriented ~N-S. Stations located just east of the Colima rift and south of the Chapala-Tula rift (CTR), however, show fast axes rotated to ~NE-SW and ~ENE-WSW. Interestingly, the fast axes at the northernmost stations MA16, MA23, and MA27, just south of the CTR, agree with the measurements at MOIG located at about the same latitude but ~200 km farther east (Figure 7), which might suggest a consistent trend for stations within the TMVB east of Colima rift.

A single splitting measurement at CUIG (38±55°, 1.20±1.25 s) is poorly constrained but its large 95% confidence interval is consistent with nearby stations in the northern segment of the MASE deployment where the fast direction is oriented slightly west of north (Rojo-Garibaldi, 2012). Station TEIG was installed in the Yucatán peninsula and is found in an entirely different tectonic setting. The fast axis here agrees with the APM of North America and is consistent with its location away from current plate boundaries.

Station ZAIG in the Mesa Central

ZAIG is the northernmost station in the present study (Figure 1). The SSN coverage in this part of the country is sparse since it is far away from the seismogenic plate boundaries. The fast axis is oriented WNW-ESE and is clearly different from that observed in any of the other stations analyzed. The station is located within the Mesa Central, which is an elevated plateau and is recognized as a morphotectonic province. It is bounded to the south by the TMVB, to the west by the Sierra Madre Occidental, and to the north and east by the Sierra Madre Oriental (SMOr), which separates it from the Eastern Mexican

Basin and Range farther north (Sedlock *et al.,* 1993). The Mesa Central was under compression during the Laramide orogeny which created the SMOr to the east (Nieto-Samaniego *et al.,* 2005). It was subsequently subjected to extension, likely related to the Basin and Range. The main episodes of extension occurred during the Eocene, oriented NE-SW; and during the Oligocene, with predominant extension of ~20% oriented E-W plus ~10% extension oriented N-S (Nieto-Samaniego *et al.,* 2005). Neither the episodes of compression nor extension can explain the orientation of ϕ. The fast axis is predicted to align parallel to transpressional structures, and parallel to the extension direction (Silver, 1996). The APM of North America cannot explain the orientation of ϕ either (Figure 1). It should be mentioned that in the Western Mexican Basin and Range the direction of ϕ is consistent with both the current APM of North America and with extension during the Miocene (Obrebski *et al.,* 2006; van Benthem *et al.,* 2008). Comparison with the Rayleigh wave model of Stubailo *et al.* (2012) shows that ZAIG is located in their low resolution area. It is nonetheless interesting that the fast direction in their model at periods from 44 to 85 s agrees with the fast direction observed in the present study.

Another possibility for explaining the anisotropy at ZAIG is to look at the evolution of the subducted slab in the mantle. The *P* wave velocity tomographic model of Yang *et al.* (2009) can image the subducted Rivera plate down to depths of ~350 km. They speculate that the leading edge of the slab may have detached from the upper portion and might be found at greater depths. Likewise, the adjacent Cocos slab to the east can be followed as a continuous feature from the surface down to a depth of ~400 km, which is the lower limit of their model. The *S* wave velocity tomographic model of van der Lee and Nolet (1997a, 1997b) images the broken and subducted Farallon plate in the upper mantle. The slab shows roughly a WNW-ESE trend, which agrees with the fast anisotropy axis at ZAIG. The southernmost extent of the Farallon slab at a depth of ~350 km is located underneath station ZAIG. Being at such a great depth it is unclear, however, how the slab might control the anisotropy observed at ZAIG. On the other hand, the *P* wave velocity tomography of Gorbatov and Fukao (2005) shows the Farallon slab under ZAIG at a depth of ~400 km, but it trends roughly E-W.

Conclusions

The fast anisotropy polarization directions for stations located where the Cocos plate subducts subhorizontally, beneath Guerrero and Oaxaca states, are oriented with the relative motion between the Cocos and North American plates and are perpendicular to the Middle America Trench. This observation is consistent with subslab entrained flow in a regime of type-A olivine. The situation is similar to that reported in Cascadia, except that the slab is not subhorizontal. At most subduction zones around the world, however, ϕ is trench-parallel, which may be caused by a thin asthenospheric layer that decouples the downgoing slab from the subslab mantle and allows flow to be driven by trench migration. Given the young age of the lithosphere being subducted, both in Mexico and in Cascadia, the decoupling layer may be absent. The fast directions observed around the edges of the Rivera slab, and near the projection of the Orozco Fracture Zone under the continent, are consistent with mantle flow around the edges of the torn slabs. Furthermore, this flow is driven by slab rollback. Stations located east of the subhorizontal slab, where the subducting plate starts to increase its dip, show a slight clockwise rotation of their fast axes relative to nearby stations located to the west. A few stations in or near the TMVB, and away from the plate boundaries, show fast directions consistent with asthenospheric flow driven by the absolute motion of the North American plate. The same is also true for one station in the Yucatán peninsula. Finally, the fast polarization direction for a single station within the Mesa Central is oriented WNW-ESE and it is different from measurements at any of the other stations. Previous episodes of compression and subsequent extension in the region fail to account for this direction. The fast direction is also inconsistent with the APM of North America.

Bibliography

Abt D.L., Fischer K.M., Abers G.A., Strauch W., Protti J.M., González V., 2009, Shear wave anisotropy beneath Nicaragua and Costa Rica: Implications for flow in the mantle wedge, *Geochem. Geophys. Geosyst.,* 10, Q05S15, doi:10.1029/2009GC002375.

Abt D.L., Fischer K.M., Abers G.A., Protti M., González V., Strauch W., 2010, Constraints on upper mantle anisotropy surrounding the Cocos slab from *SK(K)S* splitting, *J. Geophys. Res.,* 115, B06316, doi:10.1029/2009JB006710.

Bernal-Díaz A., Valenzuela-Wong R., Pérez-Campos X., Iglesias A., Clayton R.W., 2008, Anisotropía de la onda *SKS* en el manto superior debajo del arreglo VEOX (abstract), *Geos Boletín Informativo de la UGM,* 28, 2, 199-200.

Currie C.A., Cassidy J.F., Hyndman R.D., Bostock M.G., 2004, Shear wave anisotropy beneath the Cascadia subduction zone and western North American craton, *Geophys. J. Int.,* 157, 341-353.

DeMets C., Gordon R.G., Argus D.F., 2010, Geologically current plate motions, *Geophys. J. Int.,* 181, 1-80.

Dougherty S.L., Clayton R.W., Helmberger D.V., 2012, Seismic structure in central Mexico: Implications for fragmentation of the subducted Cocos plate, *J. Geophys. Res.,* 117, B09316, doi:10.1029/2012JB009528.

Ferrari L., 2004, Slab detachment control on mafic volcanic pulse and mantle heterogeneity in central Mexico, *Geology,* 32, 77-80, doi:10.1130/G19887.1.

Ferrari L., Petrone C.M., Francalanci L., 2001, Generation of oceanic-island basalt-type volcanism in the western Trans-Mexican volcanic belt by slab rollback, asthenosphere infiltration, and variable flux melting, *Geology,* 29, 507-510.

Gorbatov A., Fukao Y., 2005, Tomographic search for missing link between the ancient Farallon subduction and the present Cocos subduction, *Geophys. J. Int.,* 160, 849-854.

Gripp A.E., Gordon R.G., 2002, Young tracks of hotspots and current plate velocities, *Geophys. J. Int.,* 150, 321-361.

Heuret A., Lallemand S., 2005, Plate motions, slab dynamics and back-arc deformation, *Phys. Earth Planet. Int.,* 149, 31-51, doi:10.1016/j.pepi.2004.08.022.

Husker A., Davis P.M., 2009, Tomography and thermal state of the Cocos plate subduction beneath Mexico City, *J. Geophys. Res.,* 114, B04306, doi:10.1029/2008JB006039.

Jung H., Katayama I., Jiang Z., Hiraga T., Karato S., 2006, Effect of water and stress on the lattice-preferred orientation of olivine, *Tectonophysics,* 421, 1-22.

Kanjorski M.N., 2003, Cocos plate structure along the Middle America subduction zone off Oaxaca and Guerrero, Mexico: Influence of subducting plate morphology on tectonics and seismicity, Ph. D. thesis, University of California, San Diego, USA.

Kim Y., Clayton R.W., Keppie F., 2011, Evidence of a collision between the Yucatán block and Mexico in the Miocene, *Geophys. J. Int.,* 187, 989-1000, doi: 10.1111/j.1365-246X.2011.05191.x.

León-Soto G., González-López A., Valenzuela-Wong R., Pérez-Campos X., Iglesias A., Clayton R.W., 2011, Anisotropía sísmica de ondas *S* locales en el Istmo de Tehuantepec (abstract), *Geos Boletín Informativo de la UGM,* 31, 1, 117.

Long M.D., 2010, Frequency-dependent shear wave splitting and heterogeneous anisotropic structure beneath the Gulf of California region, *Phys. Earth Planet. Int.,* 182, 59-72, doi:10.1016/j.pepi.2010.06.005.

Long M. D., Silver P. G., 2008, The subduction zone flow field from seismic anisotropy: A global view, *Science,* 319, 315-318.

Long M.D., Silver P.G., 2009, Mantle flow in subduction systems: The subslab flow field and implications for mantle dynamics, *J. Geophys. Res.,* 114, B10312, doi:10.1029/2008JB006200.

Manea M., Manea V. C., Ferrari L., Kostoglodov V., Bandy W. L., 2005, Tectonic evolution of the Tehuantepec ridge, *Earth Planet. Sci. Lett.,* 238, 64-77.

Melgar D., Pérez-Campos X., 2011, Imaging the Moho and subducted oceanic crust at the Isthmus of Tehuantepec, Mexico, from receiver functions, *Pure Appl. Geophys.,* 168, 1449-1460, doi:10.1007/s00024-010-0199-5.

Neumann F., Contreras-Pérez J., Tolson-Jones G., Vásquez-Serrano A., 2012, An analog model of the Middle American subduction zone and the mantle flow beneath the Jalisco and Michoacán blocks (abstract), *Geos Boletín Informativo de la UGM,* 32, 1, 252.

Nieto-Samaniego A.F., Alaniz-Alvarez S.A., Camprubí-í-Cano A., 2005, La Mesa Central de México: Estratigrafía, estructura y evolución tectónica cenozoica, *Bol. Soc. Geol. Mex.,* LVII, 285-318.

Obrebski M., Castro R.R., 2008, Seismic anisotropy in northern and central Gulf of California region, Mexico, from teleseismic receiver functions and new evidence of possible plate capture, *J. Geophys. Res.,* 113, B03301, doi:10.1029/2007JB005156.

Obrebski M., Castro R.R., Valenzuela R.W., van Benthem S., Rebollar C.J., 2006, Shear-wave splitting observations at the regions of northern Baja California and southern Basin and Range in Mexico, *Geophys. Res. Lett.,* 33, L05302, doi:10.1029/2005GL024720.

Pardo M., Suárez G., 1995, Shape of the subducted Rivera and Cocos plates in southern Mexico: Seismic and tectonic implications, *J. Geophys. Res.,* 100, 12,357-12,373.

Park J., Levin V., 2002, Seismic anisotropy: Tracing plate dynamics in the mantle, *Science,* 296, 485-489.

Pérez-Campos X., Kim Y., Husker A., Davis P.M., Clayton R.W., Iglesias A., Pacheco J.F., Singh S.K., Manea V.C., Gurnis M., 2008, Horizontal subduction and truncation of the Cocos plate beneath central Mexico, *Geophys. Res. Lett.,* 35, L18303, doi:10.1029/2008GL035127.

Pérez-Campos X., Clayton R.W., Brudzinski M.R., Cabral E., Arciniega A., 2012, Slab geometry under Oaxaca and its relationship with the eastern Trans-Mexican Volcanic Belt (abstract), *Geos Boletín Informativo de la UGM,* 32, 1, 254.

Phipps Morgan J., Hasenclever J., Hort M., Rüpke L., Parmentier E.M., 2007, On subducting slab entrainment of buoyant asthenosphere, *Terra Nova,* 19, 167-173, doi:10.1111/j.1365-3121.2007.00737.x.

Rodríguez-Pérez Q., 2007, Estructura tridimensional de velocidades para el sureste de México, mediante el análisis de trazado de rayos sísmicos de sismos regionales, M.

Sc. thesis, 83 pp., Instituto de Geofísica, Universidad Nacional Autónoma de México, Mexico City, Mexico.

Rojo-Garibaldi B., 2012, Anisotropía de las ondas *SKS* en el manto superior debajo de un arreglo sísmico entre Guerrero y Veracruz, B. Sc. thesis, 84 pp., Facultad de Ciencias, Universidad Nacional Autónoma de México, Mexico City, Mexico.

Savage M.K., 1999, Seismic anisotropy and mantle deformation: What have we learned from shear wave splitting?, *Rev. Geophys.,* 37, 65-106.

Sedlock R.L., Ortega-Gutiérrez F., Speed R.C., 1993, *Tectonostratigraphic terranes and tectonic evolution of Mexico, Special Paper 278,* 146 pp., Geological Society of America, Boulder, Colorado, USA.

Silver P.G., 1996, Seismic anisotropy beneath the continents: Probing the depths of Geology, *Annu. Rev. Earth Planet. Sci.,* 24, 385-432.

Silver P.G., Chan W.W., 1991, Shear wave splitting and subcontinental mantle deformation, *J. Geophys. Res.,* 96, 16,429-16,454.

Singh S.K., Pacheco J., Courboulex F., Novelo D.A., 1997, Source parameters of the Pinotepa Nacional, Mexico, earthquake of 27 March, 1996 (M_w = 5.4) estimated from near-field recordings of a single station, *J. Seismol.,* 1, 39-45.

Song T.-R. A., Kim Y., 2012a, Anisotropic uppermost mantle in young subducted slab underplating central Mexico, *Nat. Geosci.,* 5, 55-59, doi:10.1038/ngeo1342.

Song T.-R. A., Kim Y., 2012b, Localized seismic anisotropy associated with long-term slow-slip events beneath southern Mexico, *Geophys. Res. Lett.,* 39, L09308, doi:10.1029/2012GL051324.

Soto G.L., Ni J.F., Grand S.P., Sandvol E., Valenzuela R.W., Guzmán Speziale M., Gómez González J.M., Domínguez Reyes T., 2009, Mantle flow in the Rivera-Cocos subduction zone, *Geophys. J. Int.,* 179, 1004-1012, doi: 10.1111/j.1365-246X.2009.04352.x.

Stubailo I., Davis P., 2007, Shear wave splitting measurements and interpretation beneath Acapulco-Tampico transect in Mexico, *Eos Trans. AGU,* 88, 52, Fall Meet. Suppl., Abstract T51B-0539.

Stubailo I., Davis P.M., 2012a, Anisotropy of the Mexico subduction zone based on shear-wave splitting analysis (abstract), *Seism. Res. Lett.,* 83, 2, 379.

Stubailo I., Davis P.M., 2012b, Anisotropy of the Mexico subduction zone based on shear-wave splitting and higher modes analysis, Abstract T11A-2538 presented at 2012 Fall Meeting, AGU, San Francisco, CA, 3-7 Dec.

Stubailo I., Beghein C., Davis P.M., 2012, Structure and anisotropy of the Mexico subduction zone based on Rayleigh-wave analysis and implications for the geometry of the Trans-Mexican Volcanic Belt, *J. Geophys. Res.,* 117, B05303, doi:10.1029/2011JB008631.

van Benthem S.A.C., Valenzuela R.W., Obrebski M., Castro R.R., 2008, Measurements of upper mantle shear wave anisotropy from stations around the southern Gulf of California, *Geofís. Int.,* 47, 127-143.

van der Lee S., Nolet G., 1997a, Seismic image of the subducted trailing fragments of the Farallon plate, *Nature,* 386, 266-269.

van der Lee S., Nolet G., 1997b, Upper mantle *S* velocity structure of North America, *J. Geophys. Res.,* 102, 22,815-22,838.

Wessel P., Smith W.H.F., 1998, New, improved version of Generic Mapping Tools released, *Eos Trans. AGU,* 79, 579.

Wolfe C.J., Silver P.G., 1998, Seismic anisotropy of oceanic upper mantle: Shear wave splitting methodologies and observations, *J. Geophys. Res.,* 103, 749-771.

Yang T., Grand S.P., Wilson D., Guzmán-Speziale M., Gómez-González J.M., Domínguez-Reyes T., Ni J., 2009, Seismic structure beneath the Rivera subduction zone from finite-frequency seismic tomography, *J. Geophys. Res.,* 114, B01302, doi:10.1029/2008JB005830.